Supporting Information

Rognoni et al. 10.1073/pnas.1211274109

SI Materials and Methods

Molecular Cloning. All protein constructs were inserted between two ubiquitin domains with terminal cysteines using molecular cloning techniques and expressed in *Escherichia coli*. The ubiquitins serve as spacer molecules to prevent direct reaction of the terminal cysteines later used for DNA handle coupling. Because ubiquitin domains are mechanically much more stable than Ig domains (1), they do not unfold at our exerted force range and thus do not interfere during the single-molecule mechanical measurements.

To study the binding site of domain 21 of human filamin A, the corresponding 13- to 15-aa-long binding regions of GPIbα, Migfilin, and ITβ7 were tethered to the N terminus of domain 21 via a flexible 6-aa glycine–serine linker. The resulting amino acid sequences are the following.

GPIbα-FLNa21. MACKMQIFVKTLTGKTITLEVEPSDTIENVKAKIQDKEGIPPDQQRLIFAGKQLEDGRTLSDYNIQKESTLHLVLRLRGGELGGSGG**PTFRSSLFLWVRP**GGSGGSGPLGEGGAHKVRAGGPGLERAEAGVPAEFSIWTREAGAGGLAIAVEGPSKAEISFEDRKDGSCGVAYVVQEPGDYEVSVKFNEEHIPDSPFVVPVASPSSGGSGGTMQIFVKTLTGKTITLEVEPSDTIENVKAKIQDKEGIPPDQQRLIFAGKQLEDGRTLSDYNIQKESTLHLVLRLRGGKCLEHHHHHH.

Migfilin-FLNa21. MACKMQIFVKTLTGKTITLEVEPSDTIENVKAKIQDKEGIPPDQQRLIFAGKQLEDGRTLSDYNIQKESTLHLVLRLRGGELGGSGG**PEKRVASSVFITLAP**GGSGGSGPLGEGGAHKVRAGGPGLERAEAGVPAEFSIWTREAGAGGLAIAVEGPSKAEISFEDRKDGSCGVAYVVQEPGDYEVSVKFNEEHIPDSPFVVPVASPSSGGSGGTMQIFVKTLTGKTITLEVEPSDTIENVKAKIQDKEGIPPDQQRLIFAGKQLEDGRTLSDYNIQKESTLHLVLRLRGGKCLEHHHHHH.

ITβ7-FLNa21. MACKMQIFVKTLTGKTITLEVEPSDTIENVKAKIQDKEGIPPDQQRLIFAGKQLEDGRTLSDYNIQKESTLHLVLRLRGGELGGSGG**PLYKSAITTTINP**GGSGGSGPLGEGGAHKVRAGGPGLERAEAGVPAEFSIWTREAGAGGLAIAVEGPSKAEISFEDRKDGSCGVAYVVQEPGDYEVSVKFNEEHIPDSPFVVPVASPSSGGSGGTMQIFVKTLTGKTITLEVEPSDTIENVKAKIQDKEGIPPDQQRLIFAGKQLEDGRTLSDYNIQKESTLHLVLRLRGGKCLEHHHHHH.

The bold characters denote the peptide binding regions, whereas the underlined sequence corresponds to domain 21 of human filamin A.

For investigation of the autoinhibition mechanism, the following amino acid sequence of domains 20 and 21 was used. To prevent further undesired disulfide bonds in the two-domain construct, one cysteine in domain 21 (Cys2293; all numbers are used as in the crystal structure; PDB ID code 2J3S), and two in domain 20 of human filamin A were mutated to serines (Cys2160, Cys2199).

FLNa20-21. MACKMQIFVKTLTGKTITLEVEPSDTIENVKAKIQDKEGIPPDQQRLIFAGKQLEDGRTLSDYNIQKESTLHLVLRLRGGELGGSGGSGEGRVKESITRRRRAPSVANVGSHSDLSLKIPEISIQDMTAQVTSPSGKTHEAEIVEGENHTYSIRFVPAEMGTHTVSVKYKGQHVPGSPFQFTVGPLGEGGAHKVRAGGPGLERAEAGVPAEFSIWTREAGAGGLAIAVEGPSKAEISFEDRKDGSSGVAYVVQEPGDYEVSVKFNEEHIPDSPFVVPVASPSSGGSGGTMQIFVKTLTGKTITLEVEPSDTIENVKAKIQDKEGIPPDQQRLIFAGKQLEDGRTLSDYNIQKESTLHLVLRLRGGKCLEHHHHHH.

Protein–DNA Construct Formation and DNA Handle Formation. For coupling of functionalized DNA handles, a protocol (2) derived from Cecconi et al. (3) was used. The terminal cysteines of the protein construct were activated by DTDP and mixed with TCEP-activated 3′ thiol groups of 34-bp ssDNA oligos. DNA handles of 180-nm length were generated via PCR from a lambda phage template. As forward primers, an equal mixture of biotin- and digoxigenin-modified oligos was used, whereas reverse primers contained an abasic site leaving a ssDNA overhang complementary to the protein-bound oligos. Mixture of the protein–oligo construct with the functionalized DNA handles leads to the desired DNA–protein construct. The additional reaction step including the oligos increases the DNA–protein coupling efficiency.

Optical Tweezers Setup. For the single-molecule mechanical measurements, an in-house custom-built dual-beam optical tweezers setup with back focal plane detection and one AOD-steerable beam was used as described by Gebhardt et al. (4). Trapped beads were calibrated with the technique introduced by Tolić-Nørrelykke et al. (5). Trap stiffness could be determined with an error of ∼10% and varied between different experiments from 0.25 to 0.30 pN/nm. Data were acquired at a sampling rate of 100 kHz and averaged to 20 kHz before storage. Detailed data analysis was carried out after the experiment using the difference of both 20-kHz bead signals to increase the signal-to-noise ratio (6). The signals were corrected for both cross talk due to depolarization and proximity of the beams.

Experimental Procedure. Protein–DNA constructs were mixed with silica beads (1-μm diameter; Bangs Laboratories), which were previously covalently functionalized with anti-digoxigenin Fab fragments (Roche). These constructs were subsequently mixed with streptavidin-coated silica beads (1-μm diameter; Bangs Laboratories). Measurements were carried out at room temperature in PBS (10 mM phosphate buffer, 2.7 mM potassium chloride, and 137 mM sodium chloride, pH 7.4), with an added oxygen scavenger system (26 U/mL glucose oxidase, 17,000 U/mL catalase, 0.65% glucose). The protein–DNA coupled beads were introduced into a flow cell consisting of a coverslip attached to a glass slide via Nescofilm (Bando Chemical Industries) and pretreated with BSA (Sigma-Aldrich). Trapped beads were brought into close proximity to build a bead–DNA–protein dumbbell. Protein–DNA concentrations were adjusted to only sparsely cover the beads leading mainly to single tethered dumbbells. The trapping potentials were then separated with a constant velocity yielding force vs. extension traces or held at a constant separation to record force vs. time traces. When a dumbbell was successfully tested for single tether formation through stretch-and-relax cycles, further investigations of the reported equilibrium fluctuations followed at various constant trap positions. In the resulting force vs. time traces, the state population and dwell times were determined using hidden Markov model (HMM) analysis.

Force vs. Extension Curves. During constant velocity experiments, where the position of the steerable trapping potential is moved with a constant speed, force vs. extension curves were recorded as shown in Fig. 2 *A*, *D*, and *G*. The curve shape could be reproduced with a model describing the elasticity of a DNA–protein chain. For the low-force regime, in which the protein is still folded and all tethered ligands bound, the elasticity of the DNA handles could be modeled with an extensible worm-like chain model (eWLC). In this model, the force is given by the following:

$$F_{\mathrm{eWLC}}(d_{\mathrm{DNA}}) = \frac{k_{\mathrm{B}}T}{p_{\mathrm{DNA}}}\left(\frac{1}{4\left(1-\frac{d_{\mathrm{DNA}}}{L_{\mathrm{DNA}}}-\frac{F}{K}\right)^2}-\frac{1}{4}+\frac{d_{\mathrm{DNA}}}{L_{\mathrm{DNA}}}-\frac{F}{K}\right), \quad \textbf{[S1]}$$

with persistence length p_{DNA}, contour length L_{DNA}, elastic modulus K, and extension d_{DNA}. The fit yielded persistence lengths of ~20 nm, contour lengths of ~360 nm, and elastic moduli of ~600 pN.

After unbinding of a tethered ligand or unfolding of the protein, a flexible polypeptide chain adds to the compliance of the DNA–protein construct. To account for this, the eWLC describing the DNA with the previously determined parameters was applied in series to a worm-like chain model (WLC) (7) for the protein as follows:

$$F_{\mathrm{WLC}}(d_{\mathrm{prot}}) = \frac{k_{\mathrm{B}}T}{p_{\mathrm{prot}}}\left(\frac{1}{4\left(1-\frac{d_{\mathrm{prot}}}{L_{\mathrm{prot}}}\right)^2}-\frac{1}{4}+\frac{d_{\mathrm{prot}}}{L_{\mathrm{prot}}}\right), \quad \textbf{[S2]}$$

with persistence length p_{prot} set to 0.7 nm, contour length L_{prot}, and extension d_{prot}.

For forces over 30 pN, the trapping potentials are no longer ideally linear, leading to a slight curvature in the force extension traces. Therefore, the WLC model was applied only for forces below 30 pN.

Contour Length Increases. Unfolding or tethered ligand unbinding leads to change in contour length of a stretched polypeptide chain. For all investigated constructs, the contour length changes were determined through the contour length difference of the fitted WLC models (Table S1). The corresponding theoretical values were calculated by subtracting the contour length contribution of the final conformational state from the initial contour length. Contributions of folded parts were measured from the crystal structure of the three domains 19–21 of human filamin A (PDB ID code 2J3S). The unstructured amino acid sequence contour length was calculated by multiplying the average contour length per amino acid of 3.65 Å by the number of residues.

Constant Distance. To investigate the reported equilibrium transitions caused by the tethered ligand binding and unbinding, the trapping potentials were held at a constant separation and the bead position was recorded over time giving force vs. time traces as shown in Fig. 2 *B*, *E*, and *H*. A change of the trap separation causes a different force bias leading to a shift of the equilibrium of state population. For further analysis, the dwell times for each state were determined via a HMM analysis.

HMM Analysis. A HMM analysis was performed on the 20-kHz raw data of the difference signal to assign each data point to one of the system's two states as described by Stigler and Rief (8). In brief, the raw data (Fig. 2 *B*, *E*, and *H*, gray dots) were coarse grained into typically 200 bins, and a histogram of the smoothed data (Fig. 2 *B*, *E*, and *H*, colored lines) was calculated to identify the initial level positions (Fig. 2 *B*, *E*, and *H*, maxima of peaks in black histogram). The emission values were initialized with Gaussian representation of the states. Each iteration consisted of one pass of the forward–backward algorithm followed by a re-estimation of the emission probabilities based on the maximum state probability of each data point. During the iteration process, the emission probabilities were not constrained to Gaussian shapes any more. Iterations were repeated until only negligible numbers of data points (typically less than 0.1%) were reclassified in each step. Afterward, the lifetime distribution was computed for all assigned states and compared with single exponentials, which can be used as a measure for the performance of the algorithm. The transition probability matrix was adjusted manually to yield optimal lifetime distributions.

Transition Rates. After the state assignment by HMM analysis, the off-rates were obtained from single exponentials fitted to the lifetime distributions of each state. Because the tethered peptide binding is well-described by a two-state system, this directly gives the transition rates.

The single exponential fits were applied to normalized integrated lifetimes and took into account that events shorter than a dead time τ_{min} or longer than τ_{max} could not be observed as follows:

$$p(t) = \frac{\exp\left(-k_{\mathrm{off}}\,t\right)-\exp\left(-k_{\mathrm{off}}\,\tau_{\mathrm{min}}\right)}{\exp\left(-k_{\mathrm{off}}\,\tau_{\mathrm{max}}\right)-\exp\left(-k_{\mathrm{off}}\,\tau_{\mathrm{min}}\right)}, \quad \textbf{[S3]}$$

with τ_{max} set to the trajectory's length, whereas τ_{min} depended on the applied force bias and ranged between 200 and 800 μs. The extracted rates were afterward corrected for missed events. The whole analysis procedure is described by Stigler and Rief (8) in detail for the general case of an n-state system.

Force-Dependent Probabilities and Determination of Equilibrium Free Energies. For both states, probabilities were calculated directly as the sum of all lifetime histograms for a respective state divided by the trace length. The accuracy of this estimation is limited by the finite measurement time. Therefore, uncertainties were estimated by Monte Carlo simulations by generation of a trace ensemble based on the measured transition rates and their statistical error. The SD of probabilities obtained from the resulting trace ensemble was assigned as probability error.

In the following calculations, the system bead–DNA–protein–DNA–bead has been simplified to the equivalent system bead–DNA–protein with one effective trap stiffness. The effective bead displacement is then the sum of both bead displacements and the DNA contour length is doubled.

In our constant distance measurements, the trap distances are held constant. Every length change of the protein will be associated with a change in tension, which has to be accounted for in the following calculations. Based on the linker parameters determined by fitting Eqs. **S1** and **S2** to the stretch-and-relax curves, the energy $G_i(F_i)$ stored by the bead–DNA–protein dumbbell at a force F_i is given by the following:

$$G_i(F_i) = G_i^0 + G_{\mathrm{Bead}}(F_i) + G_{\mathrm{DNA}}(F_i) + G_{\mathrm{Protein}}(F_i), \quad \textbf{[S4]}$$

with G_i^0 the free energy of the protein in state i,

$$G_{\mathrm{Bead}}(F_i) = \frac{1}{2}x_i(F_i)F_i, \quad \textbf{[S5]}$$

the Hookean bead displacement energy,

$$G_{\mathrm{DNA}}(F_i) = \int_0^{d_{\mathrm{DNA},i}} F_{\mathrm{eWLC},i}(d_{\mathrm{DNA}})\,dd_{\mathrm{DNA}}, \quad \textbf{[S6]}$$

the entropic energy of stretching of dsDNA, and

$$G_{\mathrm{Protein}}(F_i) = \int_0^{d_{\mathrm{prot},i}} F_{\mathrm{WLC},i}(d_{\mathrm{prot}})\,dd_{\mathrm{prot}}, \quad \textbf{[S7]}$$

the entropic energy of stretching of the unfolded protein.

When the system undergoes a transition from an initial state i to final state j, the force changes from F_i to F_j and the energy difference is then given by the following:

$$\begin{aligned}\Delta G_{ij}(F_i,F_j) &= G_j(F_j) - G_i(F_i)\\ &= \Delta G^0_{ij} + \Delta G_{\text{Bead}}(F_i,F_j) + \Delta G_{\text{DNA}}(F_i,F_j)\\ &\quad + \Delta G_{\text{Protein}}(F_i,F_j).\end{aligned} \quad \textbf{[S8]}$$

Because the probabilities are related to energies according to

$$\frac{P_j(F_j)}{P_i(F_i)} = \exp\left(-\frac{\Delta G_{ij}(F_i,F_j)}{k_{\text{B}}T}\right), \quad \textbf{[S9]}$$

we can obtain the energy differences of the protein between states i and j by performing a global fit to the probability data with the following:

$$P_i(F) = \frac{1}{1+\sum_{j\neq i}\exp\left(-\dfrac{\Delta G^0_{ij} + \Delta G_{\text{DNA}}(F,F_j) + \Delta G_{\text{Protein}}(F,F_j)}{k_{\text{B}}T}\right)}, \quad \textbf{[S10]}$$

and weights equal to the inverse of the errors calculated as described before.

The experimental uncertainty of the equilibrium free energy difference ΔG^0_{ij} is dominated by the calibration error of the trap stiffness of about 10%.

Zero-Load Extrapolation of Binding Rates. Due to the well-defined linear zipping geometry of the tethered peptide constructs, the contour length increase is a well-suited reaction coordinate. The force dependence of measured binding and unbinding rates was fitted with a model introduced previously by Gebhardt et al. (4) and Schlierf et al. (9) accounting for the energy differences of the DNA linker and bead displacement between the initial open/closed state i and the transition state T as follows:

$$k_{ij}(F) = k^0_i \exp\left(-\frac{\Delta G^{\#}_{i\text{T}}(F_i,F_{\text{T}})}{k_{\text{B}}T}\right), \quad \textbf{[S11]}$$

with k^0_i the binding/unbinding rate constant at zero load used as a fit parameter. The additional activation energy under force,

$$\Delta G^{\#}_{i\text{T}} = \Delta G_{\text{Bead}}(F_i,F_{\text{T}}) + \Delta G_{\text{DNA}}(F_i,F_{\text{T}}) + \Delta G_{\text{Protein}}(F_i,F_{\text{T}}), \quad \textbf{[S12]}$$

consists of the contributions discussed previously. F_{T} denotes the force acting on the construct at the transition state T between initial state i and final state j.

The protein length change $\Delta L_{i\text{T}}$ associated with a transition from i to T defines the transition state distance measured in contour length to which the system has to contract/extend before binding/unbinding over the barrier occurs.

With this model, we can extrapolate the binding and unbinding rates of the tethered peptide to zero load over a force range of 6 pN. A standard for the applicability of this model is the fact that equilibrium free energies derived from the zero-force rates by $k_{\text{B}}T\cdot\ln\,(k^0_{\text{bind}}/k^0_{\text{unbind}})$ lie close to the measured ΔG^0 values obtained from equilibrium populations of states (Table S2). Another test for consistency is the fact that the contour length increases to the transition state, $\Delta L_{\text{open,T}}$ and $\Delta L_{\text{closed,T}}$, add up to the total contour length ΔL (Tables S1 and S2).

In case of the zero-load unbinding rate k^0_{unbind}, we can directly compare it to the off-rate determined by our single-molecule competition assay. Rates extracted from both methods are in excellent agreement (Tables S2 and S3).

Brownian Dynamics Simulations. To test the state assignment based on the HMM analysis, we performed simulations of our equilibrium measurements and afterward analyzed these with the same procedures used for the original measurements. Therefore, we simulated the thermal movement of both beads in their traps using Brownian dynamics (2, 10). Mimicking the experimental setup, the two beads were connected with a linker consisting of DNA, modeled by an eWLC (Eq. **S1**), in series with a worm-like chain term (Eq. **S2**). The contour length of the protein depended on the state (open/closed; Table S1), which was determined for each time step using a Monte Carlo generator. The transition probabilities used for the Monte Carlo generator were calculated from the rates determined in the experiment (Table S2). During the simulation, the response of the two beads to the length change of the protein was calculated using Brownian dynamics. The signal was treated as in the original experiments. Therefore, data points were taken with 100 kHz and subsequently sampled down to 20 kHz. After the simulation of a full trajectory, the sum signal of the two beads was calculated and analyzed using the HMM method. An example for such a simulated trace is shown in Fig. S6*D*.

Single-Molecule Mechanical Competition Assay. Binding and unbinding of ligands added into solution can be monitored online with the following newly developed single molecule mechanical competition assay.

A ligand is tethered as a probe to the domain containing the targeted binding site as described above. During a constant distance measurement with the tethered peptide construct, the same or a different ligand competing for the identical binding site is added into solution in a concentration around the K_{D}. In contrast to similar methods based on a fluorescent signal, we were able to measure ligand concentrations of up to 100 μM because the nonbound ligand in solution gives no mechanical signal. The trap positions were adjusted to the range where the reported equilibrium fluctuations of the tethered ligand could be observed. When the construct is in the unbound state, ligands from solution can bind the unoccupied binding site blocking it for the tethered ligand. This leads to an interruption of the tethered ligand's binding/unbinding fluctuations and the construct gets trapped in the open conformation (Fig. S3). According to its characteristic off-rate, the ligand unbinds and fluctuations of the tethered ligand start again. By increasing the trap distance, the state population equilibrium of the tethered ligand is shifted to the unbound state and the binding site gets more exposed, leading to an increased number of binding events of the ligand in solution.

Compared with ligand added into solution (1–100 μM), the tethered ligand's effective concentration (calculated from measured on-rates of tethered and nontethered ligand: ~10 mM) is at least 2 orders of magnitude higher. This correlates with a similar discrepancy in dwell times of the open state. The fluctuations of the tethered ligand are much faster than the unbinding/binding events of the solution ligands (see zoom in Fig. S3*B*). Therefore, we are able to separate between the quenched state and the force-induced fluctuations. To extract the dwell times of the fluctuating and quenched state, an HMM analysis is applied to appropriately smoothed data, where the fluctuating state is averaged to its mean position while the binding/unbinding of solution ligands are still resolved (Fig. 3 *A* and *B*, white trace). The inverse of the dwell time of the unbound state τ_{bound} corresponds directly to the force and concentration independent off-rate (Fig. 3*C*). On the other hand, the dwell time of the fluctuating state τ_{unbound} equals the product of pseudo first-order binding rate k_{on}, the concentration [ligand] and the force-dependent probability of the tethered ligand to be found in the open state $P_{\text{open}}(F)$.

$$\frac{1}{\tau_{\text{unbound}}} = k_{\text{on}} \cdot [\text{ligand}] \cdot P_{\text{open}}(F). \qquad \textbf{[S13]}$$

To extract $k_{\text{on}}, \kappa := k_{\text{on}} \cdot [\text{ligand}]$ is fitted to the measured τ_{unbound} data (Fig. 3*C*). It is important to note that $P_{\text{open}}(F)$ was already determined in previous measurements without ligand in solution (Fig. S2) and only κ is optimized during fitting. Combined with the known ligand concentration [ligand], this directly gives k_{on}. An overview of all determined rates is given in Table S2.

The accessible force range of the competition assay is limited due to the force dependence of the tethered probe peptide. At the lower limit, the tethered peptide is bound most of the time, thus blocking the binding site, and only very few binding events are observed. With increasing force, this number rises, thus improving the statistical outcome. Simultaneously, the equilibrium of the tethered ligand is shifted to the open state. Increased dwell times in the open state can cause missed binding events of ligands from solution, which have fast off-rates in the range of the force-induced off-rates. This would lead to an apparent force-dependent decrease of the off-rate. Therefore, a constant off-rate is an excellent proof that no binding events are missed.

For the analysis, the fluctuating state is treated as one level (see white traces in Figs. 3 and 4 and Fig. S2) with a mean position determined by averaging over the fluctuations. When the population distribution of the tethered ligand is shifted by force, also the average extension of the construct is shifted from the shorter closed to the longer open position, whereas the signal of the quenched state remains at the position of the open state. Thus, the signal difference between quenched and fluctuating state decreases for increasing forces (Fig. S3*B*, white traces). As a consequence, data points were only taken starting from forces where a reasonable number of binding events could be observed. At the upper limit, we chose forces that lead to a 50% opening probability of the tethered ligand to ensure an exact separation between quenched and fluctuating state.

Analysis of FLNa20-21 Opening. For the two-domain construct FLNa20-21, the probability to be in the open state $P_{\text{open}}(F)$ was determined with two independent methods.

First, the equilibrium fluctuations were directly analyzed using the HMM state assignment, as done for the tethered peptide constructs (Fig. S6 *A*–*C*). Because the analysis was carried out near the resolution limit at very low forces, we additionally tested the performance of the HMM analysis by reanalyzing data that were simulated using Brownian dynamics and a Monte Carlo model based on the parameters extracted from the original data (Fig. S6 *D*–*F*). Both the original data and the simulation are in excellent agreement, which confirms the validity of our HMM analysis for low-force conditions.

Second, the probability to be in the open state $P_{\text{open}}(F)$ could also be determined independently using the single-molecule mechanical competition assay, as shown in Fig. 4*D*. $P_{\text{open}}(F)$ is given by Eq. **S10**, and because ΔG_{DNA} and $\Delta G_{\text{Protein}}$ are given by the already determined linker parameters, only the free energy difference of the opening ΔG^0_{open} is added as fit parameter. $P_{\text{open}}(F)$ was globally fitted to several independent measurements carried out at three different concentrations. Fig. 4*D* shows the dwell times after normalization by division with $k_{\text{on}} \cdot [\text{ligand}]$, giving $P_{\text{open}}(F)$. The black line corresponds to the globally fitted $P_{\text{open}}(F)$ with a free energy of 2.8 $k_{\text{B}}T$. This agrees excellently with the value determined through the kinetic HMM analysis (3.4 $k_{\text{B}}T$; Fig. 4*D*, dashed line).

For a successful dwell time analysis, the baseline of long time traces (typically 100 s) at low forces (2–4 pN) has to be constant, as shown in Fig. 4*C*. Therefore, low-frequency drift was corrected for, by subtracting a manually adjusted spline.

1. Schlierf M, Li H, Fernandez JM (2004) The unfolding kinetics of ubiquitin captured with single-molecule force-clamp techniques. *Proc Natl Acad Sci USA* 101(19): 7299–7304.
2. Stigler J, Ziegler F, Gieseke A, Gebhardt JCM, Rief M (2011) The complex folding network of single calmodulin molecules. *Science* 334(6055):512–516.
3. Cecconi C, Shank EA, Bustamante C, Marqusee S (2005) Direct observation of the three-state folding of a single protein molecule. *Science* 309(5743):2057–2060.
4. Gebhardt JCM, Bornschlögl T, Rief M (2010) Full distance-resolved folding energy landscape of one single protein molecule. *Proc Natl Acad Sci USA* 107(5):2013–2018.
5. Tolić-Nørrelykke SF, et al. (2006) Calibration of optical tweezers with positional detection in the back focal plane. *Rev Sci Instrum* 77:103101.
6. Moffitt JR, Chemla YR, Izhaky D, Bustamante C (2006) Differential detection of dual traps improves the spatial resolution of optical tweezers. *Proc Natl Acad Sci USA* 103(24):9006–9011.
7. Bustamante C, Marko JF, Siggia ED, Smith S (1994) Entropic elasticity of lambda-phage DNA. *Science* 265(5178):1599–1600.
8. Stigler J, Rief M (2012) Hidden Markov analysis of trajectories in single-molecule experiments and the effects of missed events. *Chemphyschem* 13(4):1079–1086.
9. Schlierf M, Berkemeier F, Rief M (2007) Direct observation of active protein folding using lock-in force spectroscopy. *Biophys J* 93(11):3989–3998.
10. Manosas M, et al. (2007) Force unfolding kinetics of RNA using optical tweezers. II. Modeling experiments. *Biophys J* 92(9):3010–3021.

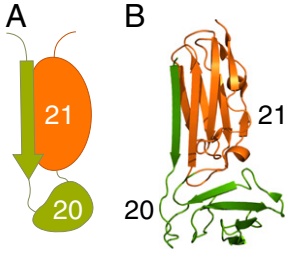

Fig. S1. Schematic representation of the structural arrangement of domains 20–21 of human filamin A. The A-strand of domain 20 is not integrated into the domain structure but binds to the subsequent domain 21. (*A*) Simplified cartoon representation used in Fig. 1*B*. (*B*) Structural representation with same coloring as in *A* based on the crystal structure with PDB ID code 2J3S (1).

1. Lad Y, et al. (2007) Structure of three tandem filamin domains reveals auto-inhibition of ligand binding. *EMBO J* 26(17):3993–4004.

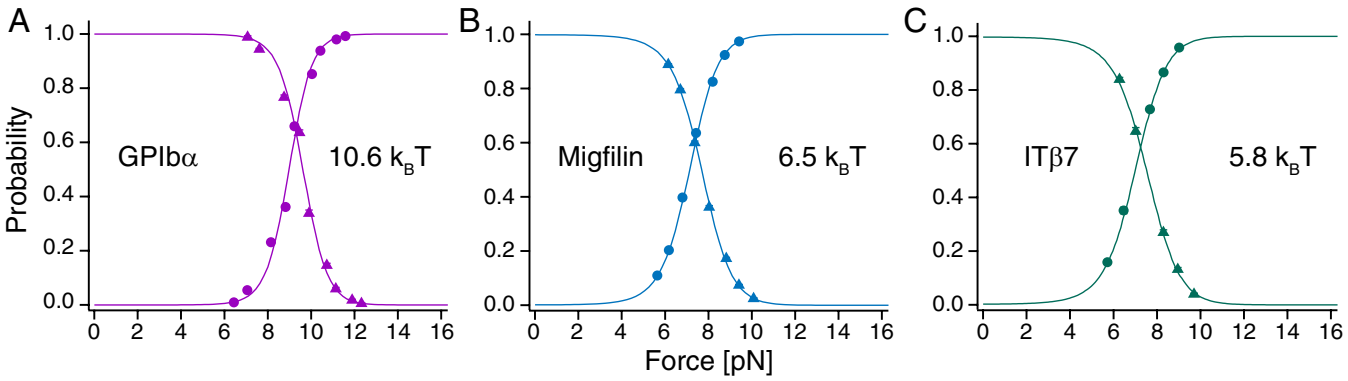

Fig. S2. Force-dependent equilibrium probabilities of tethered peptide constructs to be in the bound (triangles) or unbound (circles) state. (*A*) GPIbα-FLNa21. (*B*) Mig-FLNa21. (*C*) ITβ7-FLNa21. The solid lines correspond to the globally fitted force-dependent probability as given by Eq. **S10**. The only free fit parameter is the free binding energy of each peptide. The probabilities for the bound and unbound state do not add up to 1 because in our constant distance measurements the force is not constant for the bound and unbound state.

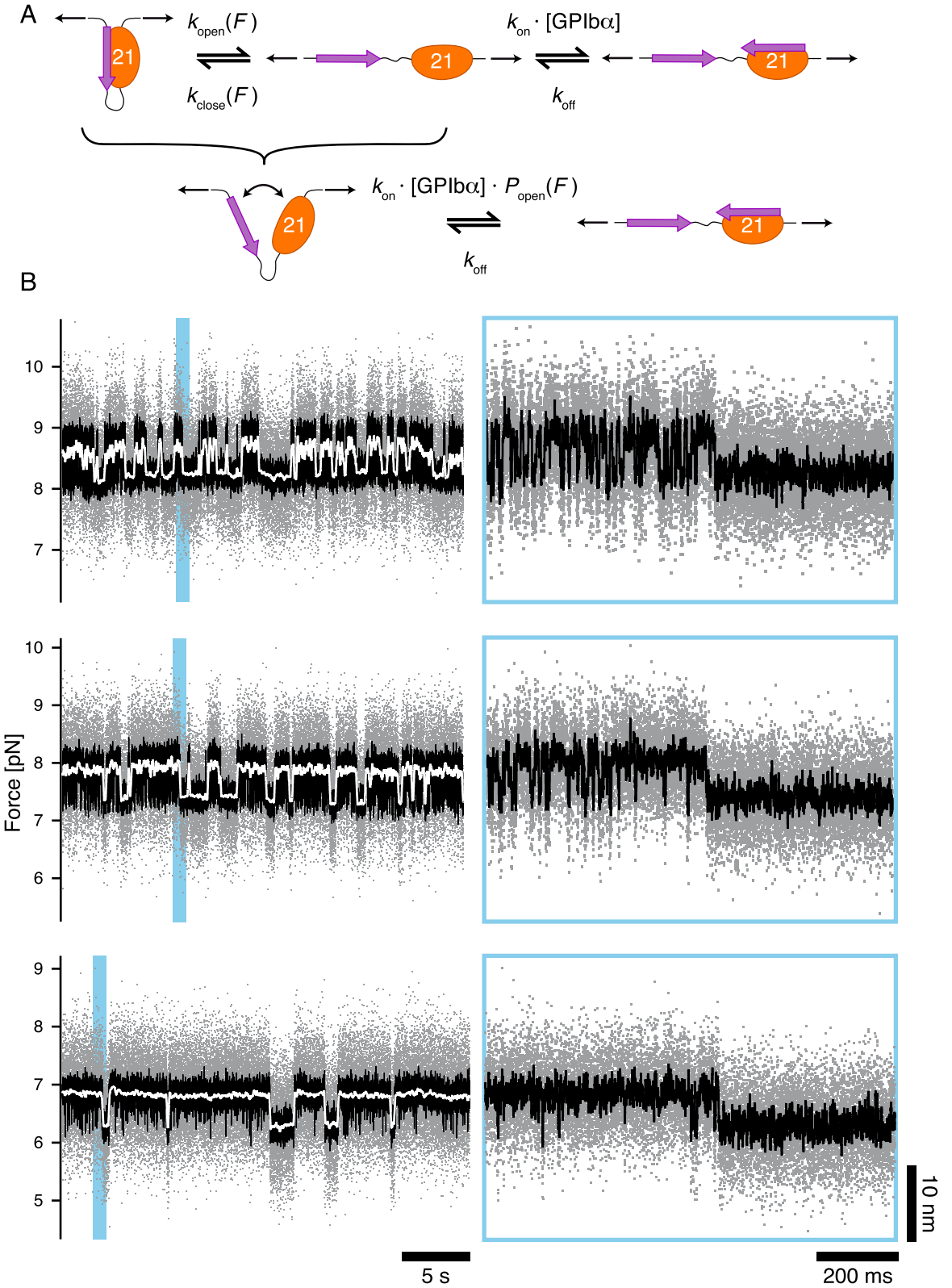

Fig. S3. Single-molecule mechanical competition assay. (*A*) Schematic representation of the rate network. The upper cartoon shows the complete network, whereas the lower represents the simplified two-state system with the fluctuating (*Left*) and quenched state (*Right*). (*B*) Three sample traces at different biasing forces. The lowest state has the smallest force and therefore the tethered probe ligand populates the bound (*Upper*) state most of the time. This can be seen in great detail in the zoom region on the right corresponding to the region marked with the light blue-filled rectangle in the left trace. Only a few quenched states are present. With increasing force (*Middle* and *Top* traces), the equilibrium of the tethered ligand is shifted more and more to the open state. Therefore, the number of quenched states increases.

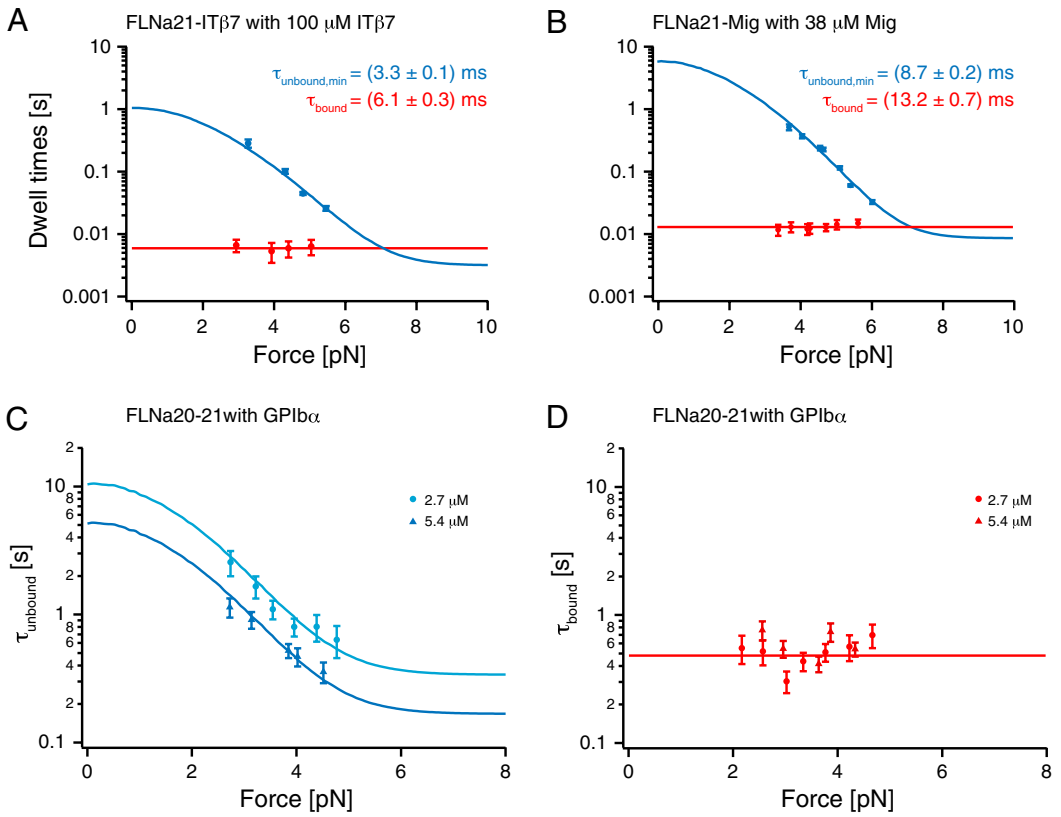

Fig. S4. Force-dependent dwell times extracted from the single-molecule mechanical competition assay. Dwell times of fluctuating (blue) and quenched (red) state of different tethered peptide constructs with corresponding peptides in solution (*A* and *B*) and of the double domain construct (FLNa20-21) with GPIbα in solution (*C* and *D*). (*A*) ITβ7 binding is measured in competition with tethered ITβ7. (*B*) Migfilin binding is measured in competition with tethered migfilin. The solid lines are fits. For the force-independent τ_{bound}, a simple line fit is used. For the force-dependent $\tau_{unbound}$, the fit is given by the inverse of Eq. **S13**. The resulting optimized fit parameters $\tau_{unbound,min}$ and τ_{bound} are shown. (*C*) Dwell times of the unbound fluctuating state of FLNa20-21 with GPIbα at two different concentrations. The solid lines are fits (compare *A* and *B*). (*D*) Dwell times of the bound or quenched state of FLNa20-21 for two different concentration of GPIbα. The solid line is a simple line fit.

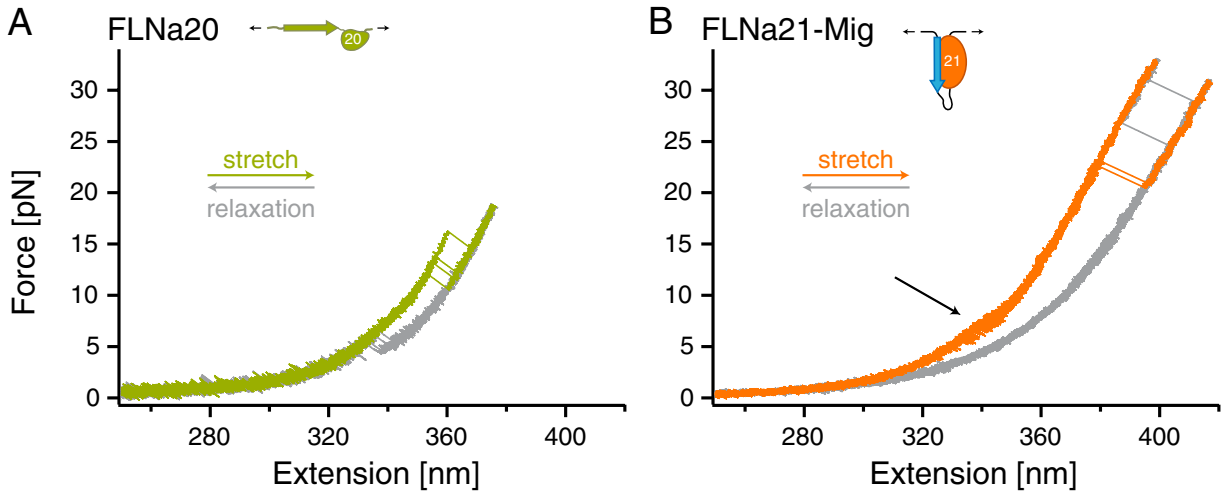

Fig. S5. Single domain force–extension curves of FLNa20 and FLNa21. The colored traces represent extension traces, whereas the gray traces show the relaxation. (*A*) Overlay of four stretch-and-relax cycles (50 nm/s) of one single domain 20 of human filamin A including the A-strand. Unfolding occurs as in the two-domain construct FLNa20-21 (Fig. 4*A*) at forces around 12 pN, suggesting that also in the single domain the A-strand is detached from the rest of the folded domain body. The gray retraction curves display refolding at forces around 5 pN. (*B*) Overlay of four complete unfolding curves of one single domain 21 of human filamin A with tethered migfilin. At low forces, the migfilin binding/unbinding fluctuations (compare Fig. 2*G*) are marked by a black arrow. At higher forces (25–30 pN) the unfolding of FLNa21 takes place as in the sample trace of the two-domain construct FLNa20-21. Furthermore, the migfilin peptide allows the demonstration that the peptide–domain interaction is specific for the folded structure of domain 21. After unfolding, the gray retraction curve shows no fluctuations compared with the extension trace at the corresponding force range around 6 pN. At zero load, the domain refolds, allowing repeated unfolding and refolding cycles with the same molecule. The mean unfolding force lies above the sampled maximal force of 35 pN. Therefore, unfolding events are rare and also happen during retraction cycles due to the slow moving speed of 10 nm/s.

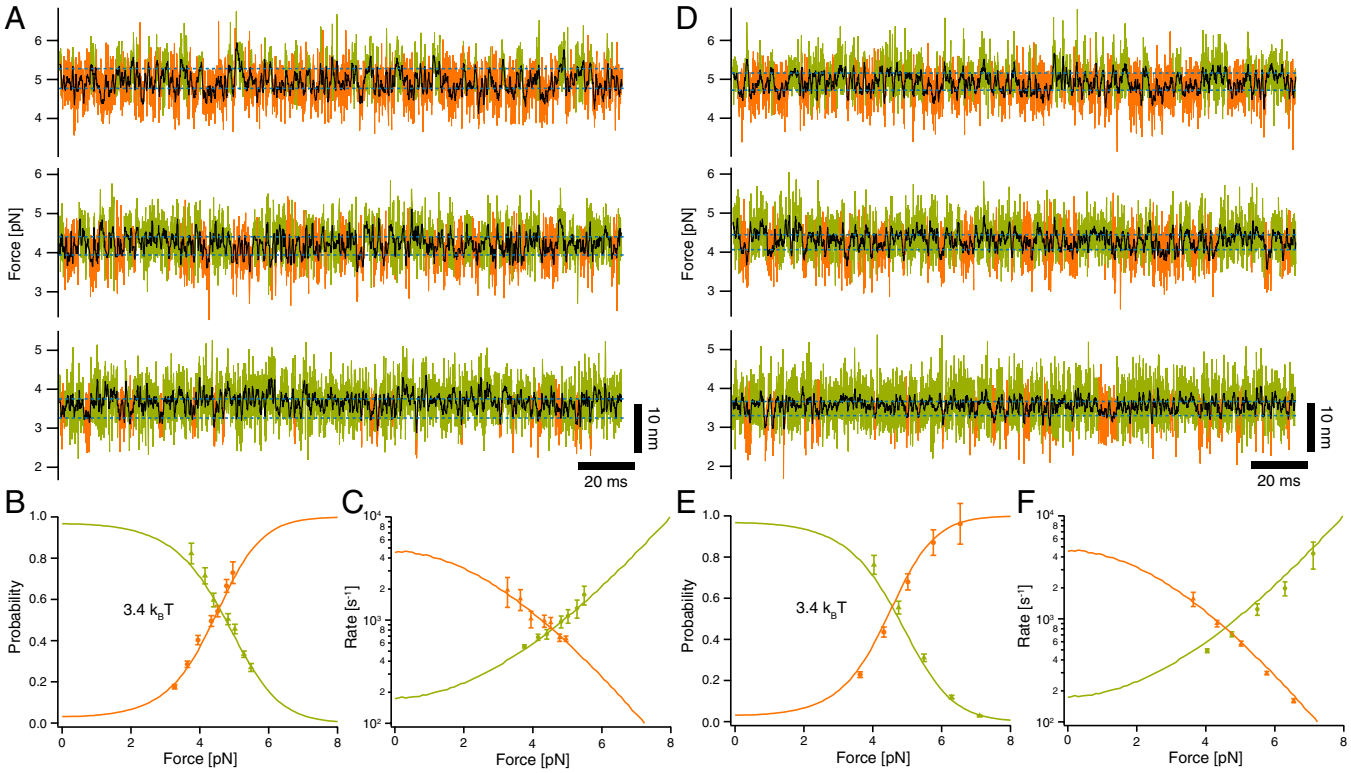

Fig. S6. Kinetic HMM analysis of opening of FLNa20-21. (*A*) Three sample traces of equilibrium measurements with HMM based assignment of the closed (*Upper*, green) and open (*Lower*, orange) state at three different biasing forces. The blue dashed lines mark state positions. The black line is a moving average of the 20-kHz data (colored lines) with 0.5-ms window size. (*B*) Force-dependent probability of the closed (green triangles) and open (orange circles) state. The solid lines are global fits to Eq. **S10** and give the equilibrium free energy difference 3.4 k_BT. Probabilities of state population do not add up to 1 due to the different forces for both states (compare with Fig. S2). (C) Force-dependent on- (orange triangles) and off-rates (green circles) of the opening and closing of the domain pair. Zero-force values are extrapolated by fits based on Eq. **S11** (solid lines). (*D–F*) Simulation of the experiment at biasing forces similar to data shown in *A*. We performed Brownian dynamics simulations of the experiment with the contour length and kinetic parameters given in Tables S1 and S2, respectively (for details, see *SI Materials and Methods*). The traces were then analyzed with our HMM analysis using the same procedure as for the original data. (*D*) Three sample traces of simulated equilibrium measurements with HMM based assignment (compare *A*). (*E*) Force-dependent probability of the simulated closed (green triangles) and open (orange circles) state. The solid lines are global fits to Eq. **S10** based on the original data shown in *B*. (*F*) Force-dependent on- (orange triangles) and off-rates (green circles) of the simulated opening and closing of the domain pair. The solid lines are the zero-force extrapolations of the original data shown in *C*. Probabilities and rate extrapolation extracted from the original data are in excellent agreement with the values extracted from the simulation.

Table S1. Contour length increases

Construct	ΔL, nm	ΔL_{calc}, nm	$\Delta L_{closed,T} + \Delta L_{open,T}$, nm
FLNa21-ITβ7	11.6 ± 0.3	11.1	9.7
FLNa21-Mig	12.0 ± 0.5	11.9	10.9
FLNa21-GPIbα	12.5 ± 0.5	11.1	12.3
FLNa20-21 opening	14.5 ± 1.1	16.8	13.7
FLNa20	17.7 ± 0.3	18.0	n.d.
FLNa21	28.8 ± 0.5	29.5	n.d.

ΔL in column 2 is the experimentally determined contour length increase using the WLC model, which was applied to force–extension traces, as well as to constant distance measurements. Errors are given as the SEM. ΔL_{calc} in column 3 are calculated contour length increases based on the crystal structure (*SI Materials and Methods*). In column 4, the sum of transition state positions (Table S2, columns 3 and 5) are given as determined by kinetic HMM analysis for constructs where equilibrium measurements were taken. For FLNa20 and FLNa21, no equilibrium measurements were done, and therefore the value is not determined.

Table S2. Rate fit parameters of tethered peptide constructs and the double domain construct

Construct	$\log_{10}(k^0_{bind})$, s^{-1}	$\Delta L_{open,T}$, nm	$\log_{10}(k^0_{unbind})$, s^{-1}	$\Delta L_{closed,T}$, nm	ΔG^0, k_BT
FLNa21-ITβ7	4.29 ± 0.20	6.5 ± 0.7	2.08 ± 0.16	3.2 ± 0.8	5.8 ± 0.6
FLNa21-Mig	4.49 ± 0.33	6.6 ± 1.1	1.78 ± 0.15	4.4 ± 0.7	6.5 ± 0.7
FLNa21-GPIbα	4.53 ± 0.21	7.7 ± 0.6	0.29 ± 0.09	4.5 ± 0.4	10.6 ± 1.1
FLNa20-21 opening	3.69 ± 0.06	7.0 ± 0.6	2.24 ± 0.01	6.7 ± 0.3	3.4 ± 0.3

All calculations are based on a model including the compliance of all mechanical elements (Eq. **S11**). Errors are given as SEM. $\Delta L_{open,T}$ and $\Delta L_{closed,T}$ are the distances from the initial closed/bound or open/unbound state to the transition state T measured in contour length (*SI Materials and Methods*). In column 6, the equilibrium free energy is given as determined by Eq. **S10**.

Table S3. Rates of peptide binding from solution measured with the single molecule mechanical competition assay

Construct	Competing peptide	Concentration, μM	k_{on}, $(\mu M*s)^{-1}$	k_{off}, s^{-1}	K_D, μM
FLNa21-ITβ7	ITβ7	50	3.03 ± 0.21	147 ± 31	48 ± 12
	ITβ7	100	3.06 ± 0.12	163 ± 4	53 ± 6
	Mig	38	3.89 ± 0.26	91.7 ± 14.1	24 ± 5
FLNa21-Mig	Mig	7.6	3.61 ± 0.13	75.2 ± 7.5	21 ± 3
	Mig	38	3.01 ± 0.08	76.0 ± 2.5	25 ± 3
FLNa21-GPIbα	GPIbα	2.3	3.57 ± 0.43	1.93 ± 0.07	0.54 ± 0.09
	GPIbα	4.7	3.83 ± 0.21	1.95 ± 0.15	0.51 ± 0.07

See *SI Materials and Methods* for details. The uncertainty of K_D in column 6 was calculated assuming a 10% maximal error for the concentration. All other errors are given as the SEM.